Journal of Testing and Evaluation

E. Lucon,[1] M. L. Martin,[2] B. L. Calvo,[3] X. Chen,[4] and M. A. Sokolov[4]

DOI: 10.1520/JTE20220691

Assessment of Different Approaches for Measuring Shear Fracture Appearance in Charpy Tests

Journal of Testing and Evaluation

doi:10.1520/JTE20220691 available online at www.astm.org

E. Lucon,[1] M. L. Martin,[2] B. L. Calvo,[3] X. Chen,[4] and M. A. Sokolov[4]

Assessment of Different Approaches for Measuring Shear Fracture Appearance in Charpy Tests

Manuscript received December 20, 2022; accepted for publication February 6, 2023; published online March 22, 2023.

[1] National Institute of Standards and Technology, 325 Broadway, Boulder, CO 80303, USA (Corresponding author), e-mail: enrico.lucon@nist.gov, https://orcid.org/0000-0002-3021-4785

[2] National Institute of Standards and Technology, 325 Broadway, Boulder, CO 80303, USA, https://orcid.org/0000-0002-5153-9597

[3] The University of Memphis, 101 Wilder Tower, Memphis, TN 38152-6400, USA

[4] Department of Materials Science and Technology, Oak Ridge National Laboratory, PO 2008 MS 6151, Oak Ridge, TN 37831-6151, USA

Reference

E. Lucon, M. L. Martin, B. L. Calvo, X. Chen, and M. A. Sokolov, "Assessment of Different Approaches for Measuring Shear Fracture Appearance in Charpy Tests," *Journal of Testing and Evaluation* https://doi.org/10.1520/JTE20220691

ABSTRACT

Different approaches for establishing shear fracture appearance (SFA) on tested Charpy specimens were assessed and compared, namely (in order of increasing expected accuracy) estimates based on characteristic forces from instrumented Charpy tests, optical measurements using image analysis software, and measurements performed with the aid of a scanning electron microscope. Comparisons between different SFA values for 129 instrumented Charpy tests currently included in the National Institute of Standards and Technology database allowed us to establish the relationships between the different available approaches and formulate recommendations for the revision of the standards ASTM E2298-18, *Standard Test Method for Instrumented Impact Testing of Metallic Materials*, and ISO 14556:2015, *Metallic Materials — Charpy V-Notch Pendulum Impact Test — Instrumented Test Method*, which currently provide four empirical correlations that can be used to estimate SFA.

Keywords

ASTM E2298, image analysis, instrumented Charpy testing, ISO 14556, scanning electron microscope, shear fracture appearance

Introduction

The most important result of a conventional Charpy test is the absorbed energy, KV, which corresponds to the work spent to fracture the specimen. It is normally calculated as the difference between initial and final potential energies of the pendulum hammer, corrected by the energy dissipated during the pendulum swing because of windage and friction. In modern machines, KV is directly returned in energy units (joules) by a digital encoder. In some older machines, an analog scale is provided, in which a pointer indicates the energy absorbed during a test.

Two additional quantities are often measured and reported:

- Lateral expansion, which corresponds to the increase in thickness of the specimen caused by plastic deformation occurring during the test
- Shear fracture appearance (SFA), which is defined as the percentage of the fracture surface that failed in a ductile (shear), or stable, manner

Although most Charpy-based codes and regulations are based on specified minimum or mean values of absorbed energy, some specifications prescribe measuring and evaluating SFA.

There are several options for measuring SFA. ASTM E23-18, *Standard Test Methods for Notched Bar Impact Testing of Metallic Materials*,[1] and ISO 148-1:2016, *Metallic Materials — Charpy Pendulum Impact Test — Part 1: Test Method*,[2] list the following five methods in order of increasing precision:

(a) Measuring by means of linear measurement tools, on the actual broken specimen, the length and width of the unstable (brittle) region and calculating the complement to 100 % with respect to the whole fracture surface
(b) Comparing the fracture surface with an SFA chart provided in ASTM E23-18
(c) Magnifying the fracture surface and comparing it with a precalibrated overlay chart or measuring SFA by means of a planimeter
(d) Photographing the fracture surface at a suitable magnification and measuring SFA by means of a planimeter
(e) Capturing a digital image of the fracture surface and measuring SFA using image analysis software

All the listed methods assume that the brittle and ductile areas are clearly distinguishable on the fracture surface, with the former ideally represented by a brittle "island" surrounded by ductile features, as in the schematic shown in **figure 1**.

Many modern alloys, however, behave significantly differently from this idealized behavior, and brittle and ductile features are intimately intermixed on the fracture surface and cannot be clearly distinguished with a straightforward optical approach. For such materials in particular and any material in general, an alternative approach can be used, based on the interpretation of the force/displacement curve of an instrumented Charpy test, as detailed in both ASTM E2298-18, *Standard Test Method for Instrumented Impact Testing of Metallic Materials*,[3] and ISO 14556:2015, *Metallic Materials — Charpy V-Notch Pendulum Impact Test — Instrumented Test Method*.[4] Specifically, values of instrumented forces at general yield (F_{gy}), maximum force (F_m), brittle fracture (F_{bf}), and crack arrest (F_a) (**fig. 2**) are used to infer values of SFA.

FIG. 1 Schematic of fracture surface for a Charpy specimen featuring both unstable and stable behavior (from ISO 148-1:2016). 1: Notch; 2: unstable (brittle) fracture; 3: stable (ductile) fracture; *A* and *B*: length and width, respectively, of the unstable fracture region.

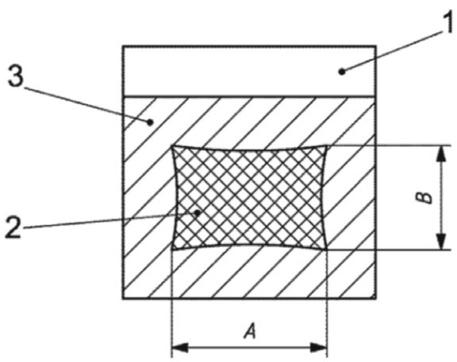

FIG. 2

Instrumented Charpy curve for a specimen tested in the ductile-to-brittle transition region, showing the force values used for estimating SFA (from ASTM E23-18[1]).

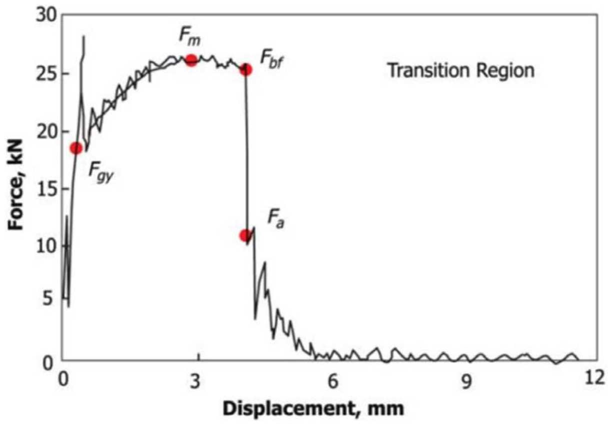

According to this approach, if there is no general yield and no crack arrest, the specimen is fully brittle and SFA = 0 %. Conversely, if there is no brittle fracture, the specimen is fully ductile and SFA = 100 %. If the specimen exhibited both stable and unstable crack propagation (ductile-to-brittle transitional behavior), an estimate of the amount of brittle fracture surface (BFA) can be obtained by comparing the magnitude of the unstable force drop ($F_{bf} - F_a$) with the maximum force F_m, generally with consideration of the plastic yielding of the ligament before maximum force ($F_m - F_{gy}$); see **figure 2**. Obviously, SFA = 100 % − BFA.

A number of such empirical correlations have been proposed in the literature,[5–11] and four of them are currently included in both ASTM E2298-18 and ISO 14556:2015:

$$\mathrm{SFA} = \left[1 - \frac{F_{bf} - F_a}{F_m}\right] \times 100\,\% \tag{1}$$

$$\mathrm{SFA} = \left[1 - \frac{F_{bf} - F_a}{F_m + (F_m - F_{gy})}\right] \times 100\,\% \tag{2}$$

$$\mathrm{SFA} = \left[1 - \frac{F_{bf} - F_a}{F_m + 0.5(F_m - F_{gy})}\right] \times 100\,\% \tag{3}$$

$$SFA = \left[1 - \sqrt{\frac{\frac{F_{gy}}{F_m} + 2}{3}} \times \left(\sqrt{\frac{F_{bf}}{F_m}} - \sqrt{\frac{F_a}{F_m}}\right)\right] \times 100\,\% \tag{4}$$

Equation (1) does not account for general yielding,[6] whereas equation (4) appears to be based on a pure empirical fit of experimental data.[9] Equation (3) was specifically developed on nuclear reactor pressure vessel steels.[8] In both standards, the precision of the SFA estimates obtained from these correlations is reported as ±20 %.

In a previously published National Institute of Standards and Technology (NIST) investigation,[12] SFA values obtained from optical measurements (method [e] in the aforementioned list) and instrumented force-based estimates were compared for nine steels of significantly different toughness (KV = 22–440 J at 21°C). Some of these materials (three different pipeline steels, duplex stainless steel) were particularly difficult to examine optically because of the intricate nature of the fracture surface microstructure when tested in the transition region. Specifically, it was found that ductile features were generally contained in unstable fracture regions but they were extremely difficult to clearly identify by optical measurements (as will be shown in the section "Details about SFA_{SEM} Measurements"). An additional outcome from this study was that the duplex stainless steel was also difficult to assess from the instrumented force-deflection curve because this was characterized by multiple small force drops, which could not be easily distinguished from dynamic force oscillations associated with hammer vibrations.

A more recent paper[13] examined the effect of various tempering temperatures on the transitional behavior of a Ni-Cr-Mo alloy steel (AISI 9310), currently used by NIST to produce super-high energy-certified reference Charpy specimens. In this investigation, a new approach was used to measure SFA, given the difficulty in distinguishing between stable and unstable crack propagation regions using a purely optical approach on selected modern high-strength steels: for a number of Charpy specimens tested in the ductile-to-brittle transition region, SFA was assessed using a scanning electron microscope (SEM) at 30 kV by determining ductile areas of fracture based on the topography and size of the features, in addition to more subtle indicators such as depth of the feature and presence of river lines.

Within the present investigation, additional steels were tested and examined, and the results of different SFA assessment methods (optical, instrumented, SEM) were compared. The outcomes were combined with those resulting from previous studies[12,13] in order to formulate general recommendations on best practices for measuring SFA on broken Charpy specimens and suggest possible modifications to test standards.

Materials Considered

The steels considered in McCowan, Lucon, and Santoyo,[12] for which optical measurements and instrumented estimates were examined, were the following:

- Low-energy AISI 4340
- API 5L X52
- High-energy AISI 4340
- AISI Grade 18Ni (T200) maraging
- API 5L X65
- API 5L X70
- API 5L X100
- UNS S32205 duplex stainless
- AISI 10260

As mentioned previously, AISI 9310 with different tempering treatments (four different conditions) was used in DelRio et al.,[13] where optical, instrumented, and SEM measurements of SFA were generated and compared.

In the current study, two new steels were tested and investigated:

- ASTM A302, *Standard Specification for Pressure Vessel Plates, Alloy Steel, Manganese-Molybdenum and Manganese-Molybdenum-Nickel*, alloy steel, Grade B: “older generation” nuclear pressure vessel steel
- F82H (heat: BA12): Japanese reduced-activation ferritic-martensitic steel for fusion applications.

New instrumented Charpy tests were also performed for two of the previously examined steels (low-energy AISI 4340 and API 5L X52).

Standard Charpy V-notch specimens were tested in a temperature range large enough to characterize the full transitional behavior of each steel from lower shelf (fully brittle behavior) to upper shelf (fully ductile behavior). High-quality digital pictures of the fracture surface were obtained for each specimen tested and analyzed to obtain optical SFA values (SFA_{opt}) using digital analysis software by two different users in parallel: an “expert” user, who had more than 30 years’ experience in testing and analyzing Charpy data (User A), and a “novice” user, who had no previous experience with Charpy testing (User B) and was just given basic training by User A. Furthermore, all newly generated instrumented force-displacement curves were analyzed by the same two users (A and B) to obtain force-based SFA estimates (SFA_{inst}) according to equations (1)–(4). Finally, SEM images of the fracture surfaces of selected Charpy specimens tested in the transition region were taken, and ductile and brittle fracture surface measurements were performed. The corresponding SFA measurements obtained are labeled SFA_{SEM}.

The rationale behind having SFA_{opt} and SFA_{inst} determinations performed by two users with significantly different experience levels was to establish how experience level might affect and eventually bias SFA values measured using two different approaches.

Influence of User's Experience Level

VALUES OF SFA_{opt}

Digital pictures of 58 tested Charpy specimens from 4 steels (A302B, F82H, X52, and 4340LL) were examined by User A (expert) and User B (novice) to generate SFA_{opt} values, which are compared in **figure 3**.

SFA_{opt} differences between the two users range between −7 and 10 %, with an average of 0.1 %. If only the 36 tests corresponding to the transition region are considered (0 % < SFA < 100 %), the average discrepancy becomes 0.2 %. A t-test on the two data sets at a confidence level $a = 0.05$ shows there is no statistical difference between the two measurement sets (calculated probability $p = 0.99$).

Based on these results, there is no reason to assume one set of measurements is more reliable than the other, and therefore mean values of SFA_{opt} between User A and User B were used in subsequent analyses.

CHARPY INSTRUMENTED FORCES

For the same 58 tests performed on steels A302B, F82H, X52, and 4340LL, values of F_{gy}, F_m, F_{bf}, and F_a were identified on the instrumented Charpy curves by User A (expert) and User B (novice). The same software for the analysis of instrumented Charpy tests, NICAS, developed in-house by NIST,[14] was used. User B established instrumented forces after being trained by User A. A second iteration was needed after large differences in elastic slopes and forces at general yield were observed from a first comparison. The final comparison between the two users is shown in **figure 4**.

A few relatively large differences, ranging between −9.0 and 22.2 %, were recorded, with an overall mean discrepancy value of 2.4 %. Significant disagreements were observed, particularly for values of F_{gy} and F_{bf}. This demonstrated that a minimum level of experience and expertise is required for a reliable analysis of instrumented Charpy curves, and therefore only values determined by User A were used in subsequent analyses. Novice users should be appropriately trained by more expert colleagues before performing extensive measurements of this type.

It should also be pointed out that for some materials, errors in the determination of instrumented forces might and do occur. Specifically, multiple brittle force drops corresponding to various unstable propagation events can be observed, as in the case of the duplex steel previously mentioned, and can be hard to distinguish

FIG. 3 Comparison between SFA_{opt} values measured by an expert user (A) and a novice user (B).

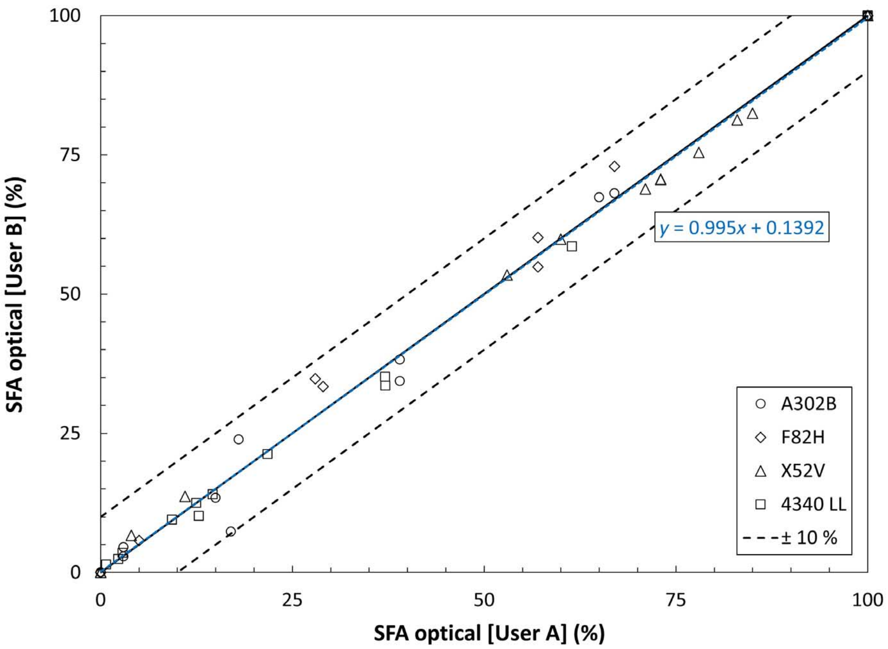

FIG. 4 Comparison between instrumented force values measured by an expert user (A) and a novice user (B).

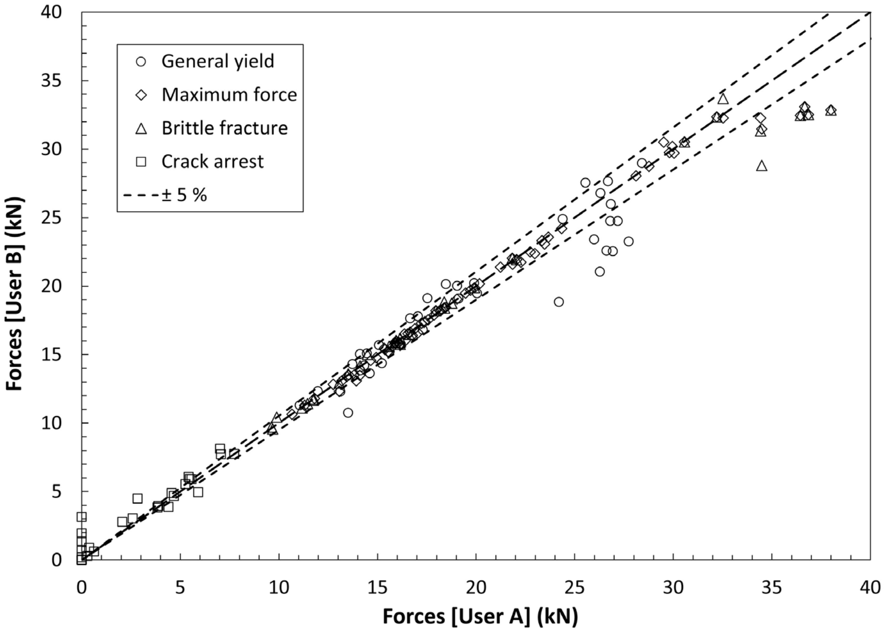

from dynamic oscillations. This might be exacerbated by insufficient resolution of the acquisition system and by the mere fact that intimately mixed fracture events cannot be clearly resolved.

Details about SFA_{SEM} Measurements

An SEM has high enough resolution to distinguish between individual fracture features such as cleavage facets (brittle) and microvoids (ductile), which are often on the scale of 10 μm. This allows for a more precise determination of what areas are composed of brittle rather than ductile fracture features. However, picking out the fine details when ductile and brittle features are intermixed needs to be balanced against capturing the scale of large features, such as the typically ductile final failure on the opposite side of the fracture surface with respect to the notch. To fully capture the fracture surface composition, the entire fracture surfaces of several samples tested in the ductile-to-brittle transition region were captured by tiling higher-magnification images; see **figure 5**. These tilings were typically around 15 by 15 images in dimension, with some variability because of the size of the shear lips. These reconstructed images of the fracture surfaces were then analyzed with image analysis software to determine the value of SFA (SFA_{SEM}).

The microscope was operated at 30 kV, the highest accelerating voltage available on the instrument, to maximize spatial resolution of the fracture features.

NIST Database of Charpy Ductile-to-Brittle Transition SFA Values

Presently, the NIST database includes SFA values for 129 Charpy specimens from 12 steels, all tested in the ductile-to-brittle transition (0 % < SFA_{opt} < 100 %). SFA_{opt} and SFA_{inst} values are available for all 129 specimens, in addition to 21 measured values of SFA_{SEM} from five steels. The whole NIST database is reproduced in the appendix.

SFA_{opt} VS. SFA_{SEM}

SEM and optical measurements of SFA are compared in **figure 6**. For 19 of the 21 data points (90 %), differences are within ±20 %. The mean difference is −2.7 %, indicating that optical measurements tend to slightly underestimate

FIG. 5 Tiled image of entire Charpy fracture surface (right) and a representative tile (left). The horizontal lines in the left image are due to slight differences in brightness/contrast of the rows of tiles. This sample was calculated to have an SFA of ~6 %. This is supported by the clear dominance of cleavage features, with some fine ductile tearing between the brittle regions. The white marks on the left hand image are dirt.

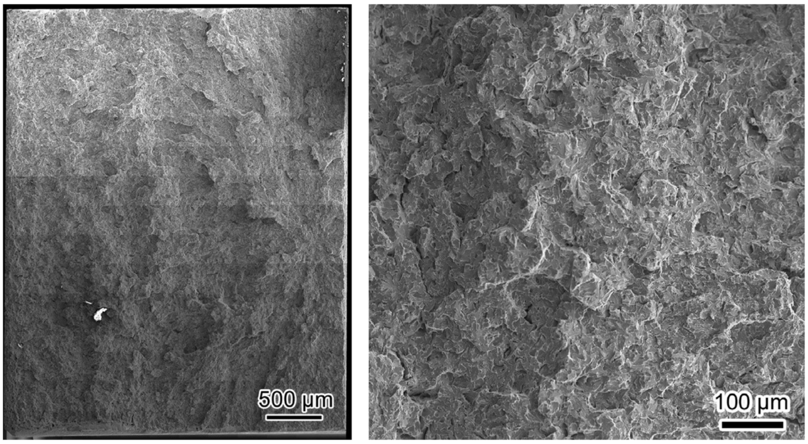

SEM measurements, as confirmed by the linear fit in **figure 6**, which also shows that the underestimation tends to increase for higher SFA values. This is not surprising, given the ability of SEM to detect smaller features: although small areas of brittle failure can be common, a more common feature that was likely missed in optical measurements was the shear failure connecting steps of regions of cleavage, leading to a slightly smaller (conservative) SFA value for optical with respect to SEM. Differences between SFA_{opt} and SFA_{SEM} range between −31.4 and 18.4 %.

Assuming that SEM values represent the "absolute reference" for SFA measurements (i.e., most accurate values), the data shown in **figure 6** substantially confirm that optical measurements can be considered reliable and can therefore be used as benchmark in the following to assess the validity of the four empirical correlations proposed by the standards.

FIG. 6

Comparison between SEM and optical SFA measurements for 21 Charpy specimens of 5 steels.

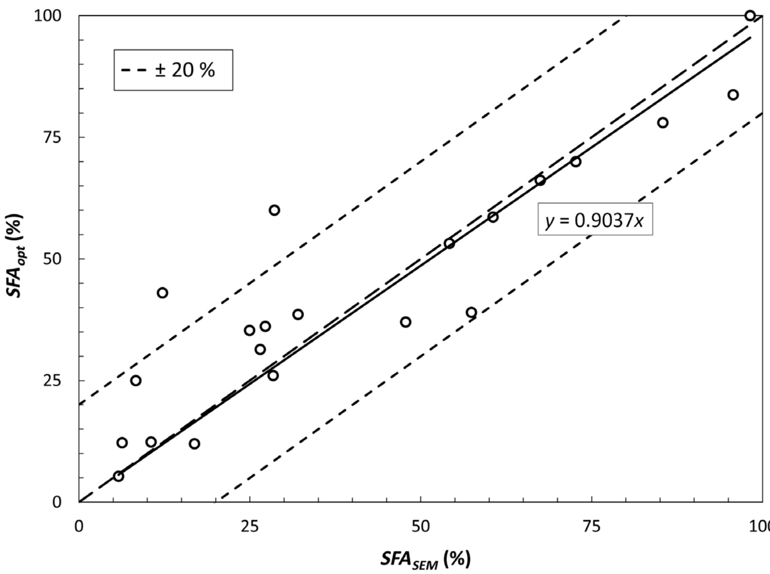

SFA_{inst} VS. SFA_{opt}

The SFA estimates obtained from the four standardized empirical correlations, equations (1)–(4), were assessed by comparison with the corresponding optical measurements for the 129 tests included in the NIST Charpy database. The reliability of each correlation was established based on a number of metrics, which are listed as follows and summarized in **Table 1**:

- $\overline{\Delta SFA}$ = mean value of $[SFA_{inst} - SFA_{opt}]$
- $SD_{\Delta SFA}$ = standard deviation of $[SFA_{inst} - SFA_{opt}]$ values
- ΔSFA_{min} = largest negative value of $[SFA_{inst} - SFA_{opt}]$
- ΔSFA_{max} = largest positive value of $[SFA_{inst} - SFA_{opt}]$
- $\Delta SFA_{max} - \Delta SFA_{\mathrm{min}}$ = range of $[SFA_{inst} - SFA_{opt}]$ values
- Correlation coefficient between SFA_{inst} and SFA_{opt}
- $\Delta SFA > \pm 20\,\%$ = number of data points outside the ±20 % error band mentioned by the standards, absolute and in percent
- Slope of a linear fit between SFA_{inst} (independent variable) and SFA_{opt} (dependent variable)

Based on the metrics presented in **Table 1**, the worst correlation is by far equation (1), which has the largest mean difference, largest range of differences, lowest correlation coefficient, and highest number of data points (23 %) outside the ±20 % error band. This correlation appears to generally underestimate the measured SFA by a significant amount, most likely because it completely ignores the contribution of the general yielding phase (between F_{gy} and F_m) to stable crack extension.

The best-performing correlation appears to be equation (2), which returned the smallest mean difference, lowest standard deviation, smallest range of differences, highest correlation coefficient, and smallest number of data points (15 %) outside the ±20 % error band. Furthermore, the slope of the linear fit between SFA_{inst} and SFA_{opt} (0.88) is the closest to unity.

Both conclusions closely match the outcome of an instrumented Charpy testing round-robin conducted by Deutsche Vertriebs und Media GmbH and reported in 1996.[11]

Optical SFA measurements from the NIST database are compared with instrumented SFA estimates in **figure 7** for equation (1) (left) and equation (2) (right), respectively the worst and the best correlation. In the lefthand side of the figure, it is evident that equation (1) is particularly inaccurate at low levels of ductility, where it returned 0 % for several specimens for which the SFA_{opt} was as high as 30 %. The same can be observed for equation (2) on the righthand side of **figure 7** but for a smaller number of specimens and for SFA_{opt} values up to ∼15 %.

The remaining two correlations, equations (3) and (4), yielded metrics relatively similar to equation (2), so they can be considered reasonable alternatives.

We also decided to look at mean estimates $\overline{SFA_{instr}}$, obtained by averaging results from all correlations $(\overline{SFA_{1,2,3,4}})$ after excluding equation (1) $(\overline{SFA_{2,3,4}})$. The metrics for the mean instrumented estimates are shown in **Table 2**, next to those for the individual correlations already shown in **Table 1**.

TABLE 1

Comparisons between SFA_{opt} and SFA_{inst} based on different metrics. The correlation that provided the best metric is marked in bold, whereas the one that provided the worst metric is shown in italic

Metric	Equation (1)	Equation (2)	Equation (3)	Equation (4)
$\overline{\Delta SFA}$, %	*−7.7*	**1.6**	−2.4	1.7
$SD_{\Delta SFA}$, %	15.8	**13.3**	14.1	*16.3*
ΔSFA_{min}, %	*−56.0*	**−39.8**	−46.8	−40.2
ΔSFA_{max}, %	**34.7**	39.5	37.4	*47.8*
$\Delta SFA_{max} - \Delta SFA_{min}$, %	*90.7*	**79.3**	84.1	88.1
Correlation coefficient	*0.88*	**0.91**	0.90	0.89
$DSFA > \pm 20$ %	*30 (23 %)*	**19 (15 %)**	20 (16 %)	28 (22 %)
Slope	0.79	**0.88**	0.84	*0.75*

FIG. 7 Comparison between SFA_{opt} and SFA_{inst} for equation (1), left, and equation (2), right.

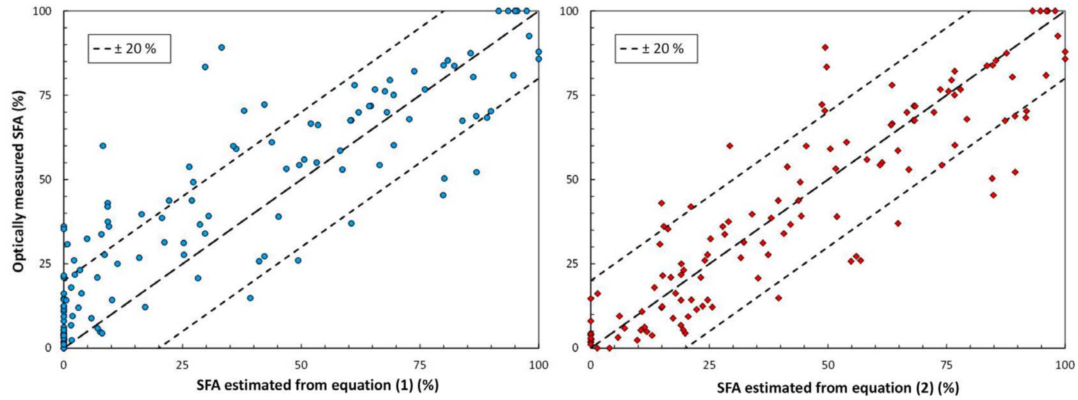

Averaging all the correlations does not bring any advantage; however, the mean estimate of equations (2)–(4) in the last column of **Table 2** provided the smallest average deviation with respect to the optical measurements (0.3 %) as well as the second smallest standard deviation and therefore appears to be a viable alternative. Comparisons between mean estimates and optical measurements are shown in **figure 8** ($\overline{SFA_{1,2,3,4}}$ on the left and $\overline{SFA_{2,3,4}}$ on the right).

TABLE 2

Comparison between SFA_{opt} and SFA_{inst} for individual correlations and mean estimates. Again, best metrics are in bold and worst are in italic

Metric	Equation (1)	Equation (2)	Equation (3)	Equation (4)	$\overline{SFA_{1,2,3,4}}$	$\overline{SFA_{2,3,4}}$
$\overline{\Delta SFA}$, %	−7.7	1.6	−2.4	1.7	−1.6	**0.3**
$SD_{\Delta SFA}$, %	15.8	13.3	14.1	*16.3*	14.3	**14.0**
ΔSFA_{min}, %	**34.7**	39.5	37.4	*47.8*	37.7	38.7
ΔSFA_{max}, %	*−56.0*	**−39.8**	−46.8	−40.2	−45.7	−42.3
$\Delta SFA_{max} - \Delta SFA_{min}$, %	*90.7*	**79.3**	84.1	88.1	83.4	81.0
Correlation coefficient	*0.88*	**0.91**	0.90	0.89	0.90	0.90
$DSFA > \pm 20$ %	*30 (23 %)*	**19 (15 %)**	20 (16 %)	28 (22 %)	21 (16 %)	20 (16 %)
Slope	0.79	**0.88**	0.84	*0.75*	0.82	0.83

FIG. 8 Comparison between SFA_{opt} and SFA_{inst} for the average of all correlations (left), and the average of equations (2)–(4) (right).

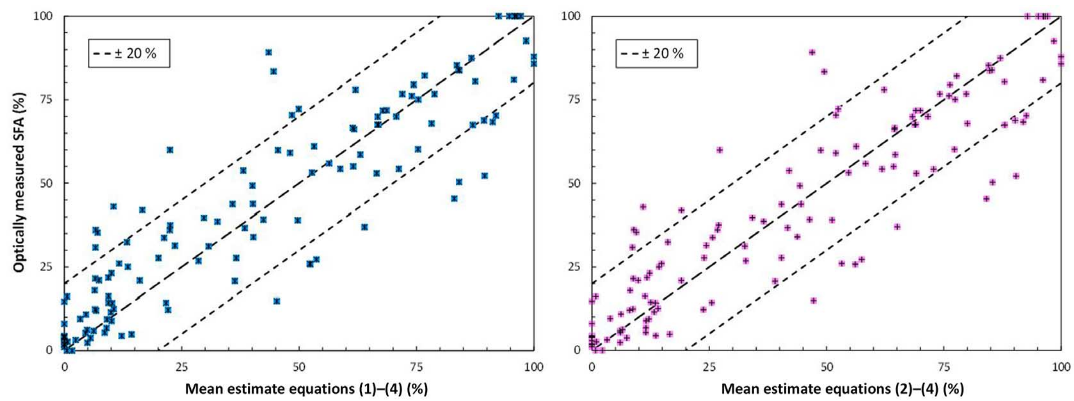

As a final observation, we remark that correlation coefficients for all equations, as well as mean estimates, are higher than 0.88. This indicates a strong degree of correlation between optical SFA measurements and instrumented estimates, irrespective of the relationship employed, and therefore justifies using this approach whenever optical measurements are difficult or highly uncertain, as can happen for some modern steels.

Conclusions and Recommendations for ASTM and ISO Standards

NIST has accumulated a database consisting of 129 instrumented Charpy tests on 12 steels with a wide range of mechanical properties, all conducted within the ductile-to-brittle transition region (i.e., neither fully brittle nor fully ductile). For all tests, optical measurements of SFA (SFA_{opt}) according to ASTM E23-18 and ISO 148-1:2016 are available as well as instrumented force-displacement curves, which allow estimating SFA based on instrumented forces (SFA_{inst}). For 21 of these tests (5 steels), SFA was measured using an SEM, which provides the most accurate measurements but represents a costly and time-consuming approach requiring adequate instrumentation and considerable operator's expertise.

Optical and SEM measurements were found in good agreement, with 90 % of the optical measurements within ±20 % of their SEM counterpart. Data indicate a slight underestimation for the optical measurements.

Systematic comparisons between optical SFA values and instrumented estimates, obtained from the four empirical correlations listed in ASTM E2298-18 and ISO 14556:2015, led to the following conclusions:

1. Regardless of the correlation employed, instrumented estimates are strongly correlated to optical measurements, justifying the use of this approach whenever optical measurements are difficult or unreliable.
2. The first correlation reported by the standards (equation (4) in ASTM E2298-18 and equation C.1 in ISO 14556:2015) is by far the least reliable because of its lack of consideration for the stable crack extension occurring during general yielding of the specimen.
3. The second correlation (equation (5) in ASTM E2298-18 and equation C.2 in ISO 14556:2015) resulted in the best performance based on most of the metrics considered in our analyses.
4. The two remaining correlations perform acceptably and provide results generally close to the second correlation, so they should be retained in the standards.
5. Averaging the estimates yielded by the second, third, and fourth correlations also represents a reliable approach, which should at least be mentioned, if not recommended, in the standards.

Therefore, based on the outcomes of our study, we recommend the following actions for the next revisions of ASTM E2298-18 and ISO 14556:2015:

- removal of the first correlation, and
- inclusion of the option of averaging the estimates from the remaining three correlations.

In the course of this investigation, we also assessed the influence of prior knowledge and expertise of the investigators by having an "expert" user and a "novice" user perform both optical SFA measurements and analyses of instrumented Charpy tests for the determination of characteristic forces (to be used in SFA estimates). Optical SFA measurements from the two users were found in excellent agreement, showing that significant expertise is not required to perform such measurements. Conversely, significant differences in the analyses of instrumented Charpy traces were observed, which highlights the importance of a minimum level of prior knowledge and experience in the analysis of instrumented Charpy traces.

ACKNOWLEDGMENTS

One of the raw materials used in this study, F82H (heat BA12), was provided by the National Institutes for Quantum and Radiological Science and Technology to Oak Ridge National Laboratory.

Appendix

NIST Database of SFA Values

TABLE A.1
SFA values for 9310, 2205 duplex steel, and mild steel

Steel	T, °C	SFA_{SEM}, %	SFA_{opt}, %	SFA_{eq4}, %	SFA_{eq5}, %	SFA_{eq6}, %	SFA_{eq7}, %	SFA_{mean_all}, %	$SFA_{mean\_5,6,7}$, %
9310	−150	16.9	12	3.1	14.9	8.7	0.5	6.8	8.0
	−75	85.4	78	61.2	63.5	61.8	61.5	62.0	62.3
	−75	8.3	25	11.3	19.1	15.4	8.4	13.5	14.3
	−25	47.8	37	60.5	64.8	62.9	67.6	63.9	65.1
	−75	57.4	39	45.2	51.9	48.8	52.9	49.7	51.2
	−25	98.2	100	97.5	97.9	97.7	95.7	97.2	97.1
	−150	12.2	43	9.2	14.9	12.1	5.7	10.5	10.9
	−90	28.4	26	49.3	56.9	52.7	50.1	52.3	53.2
2205 Duplex steel	−190		4.9	7.6	11.8	9.8	28.2	14.3	16.6
	−150		27.7	25.3	37.4	31.9	51.9	36.6	40.4
	−125		27.2	42.3	56.0	50.0	66.5	53.7	57.5
	−110		26.8	15.9	31.6	24.6	42.2	28.6	32.8
	−90		34.0	29.7	40.7	35.7	55.0	40.3	43.8
	−70		70.4	38.0	49.3	44.2	62.5	48.5	52.0
	−60		55.0	53.2	61.4	57.7	73.8	61.5	64.3
	−50		61.1	43.8	53.9	49.4	65.7	53.2	56.3
	−35		83.4	29.7	49.7	41.4	57.4	44.6	49.5
	−25		89.2	33.2	49.4	42.4	49.0	43.5	46.9
	0		92.6	98.0	98.4	98.2	98.7	98.3	98.5
	22		87.9	100.0	100.0	100.0	100.0	100.0	100.0
Mild steel	−50		0.0	0.0	1.4	0.7	0.2	0.6	0.8
	−45		0.0	0.0	4.0	2.0	0.7	1.7	2.2
	−40		9.5	1.8	6.1	4.0	1.7	3.4	3.9
	−35		10.8	0.0	10.8	5.7	2.0	4.6	6.2
	−30		16.3	3.7	17.9	11.4	4.7	9.4	11.3
	−27		21.0	0.0	16.9	9.2	3.4	7.4	9.8
	−25		21.8	2.3	19.0	11.5	4.6	9.4	11.7
	−20		23.1	3.4	19.6	12.2	5.1	10.1	12.3
	−17		36.1	9.5	27.8	19.7	32.8	22.5	26.8
	−15		33.7	7.9	28.3	19.4	29.5	21.3	25.7
	−10		37.5	9.3	29.0	20.4	31.7	22.6	27.0
	−5		39.7	16.4	34.0	26.2	42.3	29.7	34.2
	−5		43.8	27.0	43.8	36.5	53.5	40.2	44.6
	−5		43.7	22.2	39.5	31.9	49.8	35.8	40.4
	0		49.2	27.3	44.1	36.8	52.0	40.1	44.3
	5		60.2	69.5	76.7	73.6	81.5	75.3	77.3
	5		54.3	49.6	61.0	56.0	68.5	58.8	61.8
	10		76.2	67.6	75.4	72.0	80.9	74.0	76.1
	10		59.1	36.3	50.5	44.3	61.1	48.1	52.0
	12		75.1	69.4	76.7	73.6	82.0	75.4	77.4
	15		66.6	52.0	63.6	58.6	71.5	61.4	64.5
	15		83.9	80.0	84.7	82.7	88.4	83.9	85.3
	17		76.7	65.5	73.7	70.2	78.6	72.0	74.2
	17		67.9	72.7	79.3	76.5	84.4	78.2	80.0
	19		79.5	68.7	76.1	72.9	80.0	74.4	76.3
	22		85.3	80.9	85.4	83.5	84.7	83.6	84.5

TABLE A.2
SFA values for X52, X65, X70, and X100 steel

Steel	T, °C	SFA_{SEM}, %	SFA_{opt}, %	SFA_{eq4}, %	SFA_{eq5}, %	SFA_{eq6}, %	SFA_{eq7}, %	SFA_{mean_all}, %	$SFA_{mean\_5,6,7}$, %
X52	−35		6.3	0.0	11.4	6.0	2.2	4.9	6.5
	−15		16.2	0.0	1.4	0.7	0.2	0.6	0.8
	0		27.7	8.6	24.6	17.4	29.7	20.1	23.9
	10		39.2	30.5	44.4	38.2	56.6	42.4	46.4
	21		53.0	58.7	67.1	63.3	77.1	66.5	69.1
	−25	5.8	5.3	0.0	10.6	5.6	2.0	4.5	6.0
	−10	10.5	12.3	0.0	15.1	8.1	3.0	6.5	8.7
	−10		76.7	76.0	77.9	77.0	84.4	78.9	79.8
	−5	54.2	53.2	46.9	51.6	49.4	63.1	52.7	54.7
	−5		71.8	64.6	68.1	66.5	75.4	68.7	70.0
	0		71.8	64.3	68.4	66.5	72.2	67.9	69.0
	5		69.9	62.1	66.6	64.5	73.8	66.8	68.3
	22		59.9	35.7	45.4	40.9	60.0	45.5	48.8
	22	95.7	83.7	82.2	83.5	82.9	88.0	84.1	84.8
	22		82.1	73.8	76.7	75.3	81.2	76.8	77.7
X65	−90		4.4	8.0	19.9	14.4	6.5	12.2	13.6
	−65		54.3	66.5	74.0	70.7	73.7	71.2	72.8
	−50		25.8	41.1	54.9	48.9	64.6	52.4	56.1
	−35		45.4	79.9	84.9	82.7	84.7	83.0	84.1
	−20		68.4	89.1	91.7	90.6	93.5	91.2	91.9
	0		80.9	94.7	96.0	95.4	97.0	95.8	96.1
	5		85.8	100	100	100	100	100.0	100.0
X70	−150		3.9	0	0	0	0	0.0	0.0
	−125		4.4	0	0	0	0	0.0	0.0
	−112		6.8	1.5	19.0	11.1	4.4	9.0	11.5
	−99		67.4	83.9	87.3	85.8	90.9	87.0	88.0
	−98		14.3	10.2	24.6	18.0	33.9	21.7	25.5
	−90		100	95.0	96.1	95.6	96.8	95.9	96.2
X100	−149		3.9	0	0	0	0	0.0	0.0
	−90		20.7	28.2	35.3	31.9	49.9	36.3	39.0
	−80		14.9	39.3	39.6	39.4	62.7	45.2	47.2
	−75		50.3	80.1	84.6	82.6	89.0	84.1	85.4
	−70		52.2	86.9	89.5	88.3	93.4	89.5	90.4
	−50		70.3	89.9	91.9	91.0	94.9	91.9	92.6
	−50		68.8	86.8	89.4	88.3	93.0	89.4	90.2
	−35		100	95.5	96.4	96.0	97.6	96.4	96.6
	−20		100	95.1	96.0	95.6	97.2	96.0	96.3
	21		100	93.6	94.8	94.2	96.4	94.8	95.1

TABLE A.3

SFA values for 4340 low energy, 4340 high energy, T200, A302B, and F82H steel

Steel	T, °C	SFA_{SEM}, %	SFA_{opt}, %	SFA_{eq4}, %	SFA_{eq5}, %	SFA_{eq6}, %	SFA_{eq7}, %	SFA_{mean_all}, %	$SFA_{mean\_5,6,7}$, %
4340 Low energy	−198		1.7	0.0	0.0	0.0	0.0	0.0	0.0
	−150		1.9	0.0	0.0	0.0	0.0	0.0	0.0
	−121		2.6	0.1	0.1	0.1	2.7	0.7	0.9
	−90		4.2	0.0	0.0	0.0	0.0	0.0	0.0
	−60		8.0	0.0	0.0	0.0	0.0	0.0	0.0
	−30		14.7	0.0	0.0	0.0	0.0	0.0	0.0
	21		30.8	0.8	14.6	8.2	3.1	6.7	8.6
	50		42.0	9.2	21.1	15.6	20.6	16.6	19.1
	−196		1.1	0.0	0.0	0.0	0.0	0.0	0.0
	−150		2.4	1.7	9.8	5.9	2.3	4.9	6.0
	−100		3.2	0.0	5.7	2.9	1.0	2.4	3.2
	−60		9.4	0.0	20.5	11.4	4.4	9.1	12.1
	−40		11.5	0.0	22.3	12.5	4.9	9.9	13.2
	−25		12.5	0.0	23.6	13.4	5.3	10.5	14.1
	−10		14.3	0.0	21.2	11.9	4.6	9.4	12.5
	20.4		21.5	0.0	15.2	8.2	3.0	6.6	8.8
	60	27.3	36.1	0.0	15.4	8.3	3.1	6.7	8.9
	60	24.9	35.3	0.0	16.3	8.8	3.3	7.1	9.5
	110	28.6	60.0	8.2	29.3	20.1	32.3	22.5	27.3
4340 High energy	−198		5.9	7.1	7.1	7.1	3.6	6.3	6.0
	−150		8.9	5.8	17.3	12.0	5.2	10.1	11.5
	−120		18.0	1.6	13.4	7.9	3.1	6.5	8.1
	−90		72.2	42.2	48.7	45.7	63.1	49.9	52.5
T200	−198		26.0	2.2	24.0	14.5	6.0	11.7	14.8
	−150		32.4	4.9	25.2	16.3	7.0	13.4	16.2
	−120		53.8	26.4	41.4	34.8	49.9	38.1	42.0
	−90		67.6	60.5	68.0	64.7	74.4	66.9	69.0
	−60		87.5	85.7	87.7	86.7	86.8	86.7	87.0
	−30		80.4	86.2	88.9	87.7	87.2	87.5	87.9
	100		100.0	91.6	93.1	92.4	92.9	92.5	92.8
A302B	−88		2.9	0.0	0.0	0.0	0.0	0.0	0.0
	−75		3.8	0.0	12.9	6.9	2.5	5.6	7.4
	−65	6.3	12.2	17.1	25.6	21.6	24.1	22.1	23.8
	−50		14.2	0.5	19.0	10.7	10.7	10.2	13.5
	−35		20.9	7.1	23.2	15.9	18.1	16.1	19.1
	−20		36.7	28.7	42.1	36.1	46.9	38.4	41.7
	−10	32.0	38.6	20.7	38.0	30.4	41.4	32.6	36.6
	0		67.5	60.3	68.3	64.7	73.4	66.7	68.8
	10	67.5	66.2	53.5	63.3	59.0	71.1	61.7	64.5
F82H	−75		31.2	25.2	36.3	31.2	30.2	30.7	32.6
	−72		5.4	0.0	19.5	10.8	4.1	8.6	11.5
	−60	26.5	31.4	21.2	32.3	27.1	13.7	23.6	24.4
	−50		55.9	50.6	58.2	54.7	62.1	56.4	58.3
	−35	60.6	58.6	58.2	64.7	61.7	67.5	63.0	64.6
	−30	72.7	70.0	68.0	72.3	70.3	72.2	70.7	71.6

References

1. *Standard Test Methods for Notched Bar Impact Testing of Metallic Materials*, ASTM E23-18 (West Conshohocken, PA: ASTM International, approved June 1, 2018), https://doi.org/10.1520/E0023-18
2. *Metallic Materials — Charpy Pendulum Impact Test — Part 1: Test Method*, ISO 148-1:2016 (Geneva, Switzerland: International Organization for Standardization, 2016).
3. *Standard Test Method for Instrumented Impact Testing of Metallic Materials*, ASTM E2298-18 (West Conshohocken, PA: ASTM International, approved June 1, 2018), https://doi.org/10.1520/E2298-18
4. *Metallic Materials — Charpy V-Notch Pendulum Impact Test — Instrumented Test Method*, ISO 14556:2015 (Geneva, Switzerland: International Organization for Standardization, 2015).
5. D. A. Canonico, W. J. Stelzman, R. G. Berggren, and R. K. Nanstad, *Use of Instrumented Charpy Tests to Determine Onset of Upper-Shelf Energy, ORNL-5086* (Oak Ridge, TN: Oak Ridge National Laboratory, 1975).
6. *Kerbschlagbiegeversuch nach Charpy, Teil 1: Prüfverfahren* (Berlin, Germany: Deutsches Institut für Normung, 1991).
7. R. K. Nanstad and R. G. Berggren, *Irradiation Effects on Charpy Impact and Tensile Properties of Low Upper-Shelf Welds, HSSI Series 2 and 3, NUREG/CR-5696, ORNL/TM-11804* (Oak Ridge, TN: Oak Ridge National Laboratory, 1991).
8. A. Fabry, E. van Walle, R. Chaoudi, J. P. Wannijn, A. Verstrepen, J. L. Puzzolante, Th. Van Ransbeek, J. Van de Velde, and T. Petrova, "RPV Steel Embrittlement: Damage Modeling and Micromechanics in an Engineering Perspective," in *Principal Working Group No. 3 on Primary Circuit Integrity: Specialist Meeting on Irradiation Embrittlement and Optimization of Annealing - Paris (France), 20-23 September 1993* (Paris, France: Organisation for Economic Co-operation and Development, 1994), 275–353.
9. M. Nevalainen, R. Rintamaa, and K. Wallin, *Round Robin of DVM-Arbeitsgruppe instrumentierter Kerbschlagversuch: Results of the VTT Instrumented Impact Tests, VTT Metallilaboratorio, Tutkimusraportti B, no. 226* (Espoo, Finland: VTT Technical Research Centre of Finland, 1993).
10. R. K. Nanstad and M. A. Sokolov, "Charpy Impact Test Results on Five Materials and NIST Verification Specimens Using Instrumented 2-mm and 8-mm Strikers," in *Pendulum Impact Machines: Procedures and Specimens for Verification*, ed. T. A. Siewert and A. K. Schmieder (West Conshohocken, PA: ASTM International, 1995), 111–139, https://doi.org/10.1520/STP14660S
11. W. Böhme, "Experience with Instrumented Charpy Tests Obtained by a DVM Round-Robin and Further Developments," in *Evaluating Material Properties by Dynamic Testing*, ESIS 20, ed. E. Van Walle (New York: Wiley, 1996).
12. C. N. McCowan, E. Lucon, and R. L. Santoyo, "Fracture Appearance of Steels in Transition: Experimental Observations and Measurements," *Journal of Testing and Evaluation* 47, no. 2 (2019): 1009–1022, https://doi.org/10.1520/JTE20170448
13. F. W. DelRio, M. L. Martin, R. L. Santoyo, and E. Lucon, "Effect of Tempering on the Ductile-to-Brittle Transitional Behavior of Ni-Cr-Mo Low-Alloy Steel," *Experimental Mechanics* 60, no. 8 (October 2020): 1167–1172, https://doi.org/10.1007/s11340-020-00630-4
14. D. Lauria and E. Lucon, *NIST Instrumented Charpy Analysis Software (NICAS) – User's Manual, NISTIR 8302* (Gaithersburg, MD: National Institute of Standards and Technology, 2020), https://doi.org/10.6028/NIST.IR.8302